Department of Physics Papers   Department of Physics

2-3-2010

Heat Transport in Model Jammed Solids

Vincenzo Vitelli
University of Pennsylvania

Ning Xu
University of Pennsylvania, xuning@seas.upenn.edu

Matthieu Wyart
Harvard University

Andrea J. Liu
University of Pennsylvania, ajliu@physics.upenn.edu

Sidney R. Nagel
University of Chicago

Heat Transport in Model Jammed Solids

Abstract

We calculate numerically the normal modes of vibrations in three-dimensional jammed packings of soft spheres as a function of the packing fraction and obtain the energy diffusivity, a spectral measure of transport that controls sound propagation and thermal conductivity. The crossover frequency between weak and strong phonon scattering is controlled by the coordination and shifts to zero as the system is decompressed toward the critical packing fraction at which rigidity is lost. We present a scaling analysis that relates the packing fraction dependence of the crossover frequency to the anomalous scaling of the shear modulus with compression. Below the crossover, the diffusivity displays a power-law divergence with inverse frequency consistent with Rayleigh law, which suggests that the vibrational modes are primarily transverse waves, weakly scattered by disorder. Above it, a large number of modes appear whose diffusivity plateaus at a nearly constant value before dropping to zero above the localization frequency. The thermal conductivity of a marginally jammed solid just above the rigidity threshold is calculated and related to the one measured experimentally at room temperature for most glasses.

Disciplines
Physical Sciences and Mathematics | Physics

Heat transport in model jammed solids

Vincenzo Vitelli,[1] Ning Xu,[1,2] Matthieu Wyart,[3] Andrea J. Liu,[1] and Sidney R. Nagel[2]

[1]*Department of Physics and Astronomy, University of Pennsylvania, Philadelphia, Pennsylvania 19104, USA*
[2]*The James Frank Institute, The University of Chicago, Chicago, Illinois 60637, USA*
[3]*HSEAS, Harvard University, Cambridge, Massachusetts 02138, USA*

We calculate numerically the normal modes of vibrations in three-dimensional jammed packings of soft spheres as a function of the packing fraction and obtain the energy diffusivity, a spectral measure of transport that controls sound propagation and thermal conductivity. The crossover frequency between weak and strong phonon scattering is controlled by the coordination and shifts to zero as the system is decompressed toward the critical packing fraction at which rigidity is lost. We present a scaling analysis that relates the packing fraction dependence of the crossover frequency to the anomalous scaling of the shear modulus with compression. Below the crossover, the diffusivity displays a power-law divergence with inverse frequency consistent with Rayleigh law, which suggests that the vibrational modes are primarily transverse waves, weakly scattered by disorder. Above it, a large number of modes appear whose diffusivity plateaus at a nearly constant value before dropping to zero above the localization frequency. The thermal conductivity of a marginally jammed solid just above the rigidity threshold is calculated and related to the one measured experimentally at room temperature for most glasses.

I. INTRODUCTION

The thermal and mechanical properties of disordered solids can differ dramatically from those of crystalline materials [1]. Prominent among the anomalous properties are the specific heat and thermal conductivity, which display common features at subhelium to room temperatures, in amorphous materials ranging from glasses to plastics and even frozen grease [2]. This commonality suggests that the explanation of the unusual features of disordered solids may involve general physical principles that transcend detailed information about the chemical structure of specific compounds [3–5].

This paper focuses on the *intermediate* temperature regime, 1 K$< T <T_{\rm room}$. In this regime, the thermal conductivity has a plateau followed by a nearly linear rise at higher T, in contrast to the sharp drop seen in crystalline materials in the same range [6,7]. In the temperature range of this thermal-conductivity plateau, the ratio of the heat capacity $C(T)$ to the expected T^3 dependence predicted by the Debye model for crystalline solids, $C(T)/T^3$, exhibits a prominent peak, termed the boson peak, which is a hallmark of amorphous solids [2,8].

At lower temperatures, $T<1$ K, the thermal conductivity exhibits a T^2 rise, in contrast to the T^3 dependence observed in crystals [9]. Meanwhile the heat capacity increases linearly in T [2,10], in contrast to the T^3 rise predicted by Debye for long-wavelength sound modes. These low-temperature features have been rationalized by invoking the scattering of long-wavelength phonons off two-level systems, posited to arise from groups of atoms tunneling between two minima [11,12]. While this view of the low-temperature regime is widely accepted, little consensus exists regarding the intermediate temperature regime. In particular, the origin of the plateau in the thermal conductivity is controversial, and the question of whether the plateau in the thermal conductivity is linked to the boson peak remains unresolved.

In this article, we study a class of model amorphous solids composed of spherical particles interacting via a repulsive potential that vanishes at a well-defined distance corresponding to their diameter. These models possess a jamming/unjamming transition as a function of packing density [13]. Thus, the strength of the elastic moduli can be tuned continuously downwards by decreasing the density of the packing until the particles no longer interact. At that critical density, the disordered solid unjams to form a fluid. Numerical simulations have revealed the existence of a large number of vibrational modes in excess of Debye prediction whose frequency onset ω^* can be pushed to zero by decreasing the packing fraction [14]. The boson peak temperature T^* observed in the heat capacity data is controlled by $\omega^* \sim \frac{K_B T^*}{\hbar}$, the Boson peak frequency which heralds the onset of the excess vibrational modes. Similarly, to understand the plateau in the thermal conductivity and its subsequent rise, it is useful to determine the energy diffusivity, a spectral measure of energy transport that elucidates how different portions of the spectrum contribute to heat conduction.

The energy diffusivity, $d(\omega)$, quantifies how far a wave packet narrowly peaked at a frequency ω can propagate. We find that the diffusivity [15] displays a well-defined kink at a frequency ω_d that separates the low ω regime of divergent diffusivity (consistent with Rayleigh law) from a characteristic plateau that persists up to high ω where localization sets in. Numerical calculation of the vibrational density of states and the diffusivity enables us to track the pressure dependences of the boson peak frequency ω^* and the transport crossover frequency ω_d individually and to compare them. We find that ω_d and ω^* are not only comparable in magnitude, but decrease in tandem as we decrease packing fraction toward the unjamming transition. This shows that the transport crossover is linked to the excess modes.

A unique feature of disordered sphere packings is that the transport crossover frequency ω_d can be obtained perturba-

tively by means of simple scaling laws parameterized in terms of the distance from the critical unjamming transition, denoted as point J [13]. Furthermore in disordered sphere packings, some of the universal properties of amorphous solids are manifested in their most extreme form as the unjamming transition is approached. For example, in that limit the diffusivity plateau extends all the way to the lowest frequencies studied in the simulations. This suggests that in the amorphous packings studied in this work the origin of the diffusivity plateau can be traced to properties of the unjamming transition [15].

The outline of this paper is as follows. In Sec. II, we provide the necessary background on the link between vibrational dynamics and heat transport on which our work is built and review the scaling properties of jammed solids. In Sec. III, we review the methodology adopted to calculate the energy diffusivity using the Kubo formula, which enables a first-principles calculation of the diffusivity for computer-generated packings. In Sec. IV, we present our results for the transport crossover and show that this occurs at the boson peak frequency. We also present a scaling analysis that rationalizes how the main features of the diffusivity depend on the distance from the unjamming transition for both Hertzian and harmonic interactions. Section V focuses on the most striking transport signature of jammed packings: a plateau in the diffusivity as a function of frequency, whose origin we explain starting from a set of assumptions concerning the nature of the vibrational modes above the transport crossover. The ac thermal conductivity at point J is then obtained in Sec. VI. In Sec. VII we conclude by summarizing the broader message of this article: the thermal conductivity of various amorphous materials under pressure can be explained from the vibrational modes at point J, which controls energy transport at higher densities in the manner expected for a critical point.

II. BACKGROUND

Several theoretical models have been advanced to explain the boson peak, starting from distinct physical mechanisms such as the existence of resonant (quasi)localized modes [16–20], anharmonic interactions induced by the presence of defects [21,22], the breakdown of continuum elasticity below a characteristic length scale [23,24] or quenched disorder in the elastic constants [25–27]. Some of these models find that the onset of the excess vibrational modes coincides with a crossover from weakly scattered plane waves to strongly scattered vibrational modes that are delocalized and poorly conducting [28,29].

The connection between the boson peak and the transport crossover has been probed using Brillouin scattering measurements but no firm conclusion has been reached to date [30,31]. A recent experimental study suggested that the excess modes in the density of states appear when the mean free path of longitudinal phonons approaches their wavelength [32]. This condition to estimate the crossover between weak and strong scattering was also used in an independent study that challenges the previous claim by concluding instead that the criterion is satisfied only at frequencies signifi-

cantly higher than the Boson peak frequency [33]. Classic experimental studies of Raman scattering point to another important piece of experimental evidence, namely that the vibrational modes at the Boson peak are transverse in character [34,35]. This observation is supported by simulations of silica [36,37] and soft sphere glasses [38]. Recent numerical simulations provided additional evidence that suggests the equality of the Boson peak frequency with the transport crossover for transverse phonons [39].

A. Vibrational dynamics and heat transport

It was originally suggested by Kittel [40] that the intermediate temperature properties of glasses might be understood from the microscopic vibrational dynamics of amorphous materials. Instead of focusing directly on the heat capacity, $C(T)$, and thermal conductivity, $\kappa(T)$, consider the density of states, $D(\omega)$, and diffusivity, $d(\omega)$. A heuristic argument for the relation between $d(\omega)$ and $\kappa(T)$ is as follows. For a system in a temperature gradient, it is well known that the heat diffusivity obeys the relation $d = \kappa V/C$. Thus, $\kappa = dC/V$. This relation can be generalized mode by mode. Thus, the heat capacity is [4,5,41]

$$C(T) = \sum_i C(\omega_i, T), \tag{1}$$

where the sum runs over all vibrational modes i and $C(\omega_i, T)$ is the heat capacity per mode, which is obtained from the Bose-Einstein distribution and is a universal function that characterizes the heat carried by a mode of frequency ω_i at temperature T. Similarly, the thermal conductivity is

$$\kappa(T) = \frac{1}{V} \sum_i d(\omega_i) C(\omega_i), \tag{2}$$

where $d(\omega_i)$ is the energy diffusivity of mode i.

We may recast Eqs. (1) and (2) in continuum form using the density of vibrational states:

$$C(T) = \int_0^\infty d\omega D(\omega) C(\omega, T), \tag{3}$$

$$\kappa(T) = \frac{1}{V} \int_0^\infty d\omega D(\omega) d(\omega) C(\omega, T). \tag{4}$$

Both $D(\omega)$ and $d(\omega)$ are strongly *structure dependent*: the density of states and diffusivity are the fingerprints of the vibrational modes in the solid and control its heat capacity and thermal conductivity.

Inspection of Eq. (3) reveals that the prominent boson peak observed at the temperature T^* in most amorphous solids is triggered by a large number of excess vibrational modes that show up in the density of states at a characteristic frequency $\omega^* \sim \frac{K_B T^*}{\hbar}$. It is known empirically that ω^* increases as the sample is compressed [42,43], a property shared by the soft sphere packings investigated in this study. By analogy, Eq. (4) suggests that the origin of the thermal-conductivity plateau around T^* can be similarly traced to the existence of a transport crossover in $d(\omega)$ at ω^*.

At very low frequency, the diffusivity can be factored out as the product of the speed of sound v and $\ell(\omega)$ [2]:

$$d(\omega) = \frac{v}{3}\ell(\omega). \tag{5}$$

The mean free path $\ell(\omega)$ typically diverges as $\omega \to 0$ because the corresponding vibrational modes can be regarded as long-wavelength plane waves weakly scattered by disorder [44].

B. Jammed sphere packings

In order to shed some light on the pressure dependence of the density of states and energy diffusivity of disordered solids, we study a model of amorphous packings of frictionless spheres interacting via the repulsive pair potential $V(r_{ij})$

$$V(r_{ij}) = \frac{\epsilon}{\alpha}(1 - r_{ij}/\sigma_{ij})^{\alpha} \quad \text{if } r_{ij} < \sigma_{ij},$$

$$V(r_{ij}) = 0 \quad \text{if } r_{ij} > \sigma_{ij}, \tag{6}$$

where the distance between the centers of particles i and j is denoted by r_{ij} and the sum of their radii by σ_{ij}. We generate $T=0$ packings by conjugate-gradient energy minimization according to the procedure described in Ref. [13]. Irrespective of the value of α, this model system exhibits a jamming/unjamming transition at $T=0$ at a packing fraction $\phi = \phi_c$ (point J) at which the particles are just touching each other and there is no overlap [13].

The zero-temperature jamming/unjamming transition has mixed character. At this transition, the average coordination number, z, jumps [13,45] from zero to the minimum value required for mechanical stability, the "isostatic" value $z_c = 2D$ [46], where D is the dimensionality of the sample. At densities lower than ϕ_c, particles are free to rearrange while above ϕ_c at $\Delta\phi \equiv \phi - \phi_c$, the system behaves as a weakly connected amorphous solid with an average coordination number that scales as a power law with an exponent consistent with 1/2 [13,45],

$$\Delta z \equiv z - z_c \sim \Delta\phi^{1/2}. \tag{7}$$

In addition, both elastic moduli exhibit scaling behavior near the jamming point consistent with [13,45]

$$G \sim \Delta\phi^{\alpha-3/2}, \tag{8}$$

$$B \sim \Delta\phi^{\alpha-2}. \tag{9}$$

For harmonic repulsions ($\alpha=2$), the bulk modulus is independent of compression while the shear modulus vanishes as point J is approached. The bulk modulus scales as the second derivative of the potential with respect to compression, while the scaling of the shear modulus does not follow this naive scaling.

The ratio $G/B \sim \Delta\phi^{0.5}$ of the two elastic moduli is independent of α and controls the relative contribution of transverse to longitudinal waves at low frequency. This can be checked explicitly by considering that the phonon density of states at very low frequency satisfies the ubiquitous Debye law $D(\omega) \sim \frac{\omega^2}{v^3}$ except at point J where, as we shall see, the Deybe regime is completely swamped by the excess vibrational modes. The transverse and longitudinal speeds of sound v_t and v_l are proportional to the square root of the shear and bulk moduli, respectively,

$$v_t \sim \Delta\phi^{(2\alpha-3)/4}, \tag{10}$$

$$v_l \sim \Delta\phi^{(\alpha-2)/2}. \tag{11}$$

Upon substituting into the Deybe formula, $D(\omega) \sim \omega^2/v^3$, Eqs. (10) and (11) imply that the ratio of the transverse to the longitudinal density of states at low frequency, $D_t/D_l \sim \Delta\phi^{-3/4}$, becomes arbitrarily large as $\Delta\phi \to 0$. Thus, the density of states is dominated by transverse modes at low frequencies where wavelike behavior is expected, irrespective of the potential.

Numerical studies [13,14] have revealed the presence of excess vibrational modes that contribute to a plateau in the density of vibrational states above a characteristic frequency, ω^*. Close to the jamming point ω^* increases with density consistent with the power law [14]

$$\omega^* \sim \Delta\phi^{(\alpha-1)/2}. \tag{12}$$

Thus, the plateau extends to zero frequency in a marginally jammed solid (i.e., a packing of particles just above the onset of mechanical rigidity). The scaling of ω^* has been derived for systems near the isostatic jamming transition using a variational argument that predicts the presence of extended heterogeneous modes with strong spatial decorrelations [23]. This structural property suggests that the ability to transport heat for vibrational modes above ω^* should be impaired [47].

III. METHODS AND MODEL

The energy diffusivity, $d(\omega)$, introduced in Sec. II A, can be viewed physically in terms of the behavior of a wave packet narrowly peaked at a frequency ω and localized at position $\vec{r}$ at time $t=0$. The stationary value of the diffusivity, $d(\omega)$, is given by the square of the width of the wave packet at time t, divided by t at long times t [4].

If the width grows linearly in time, the diffusivity is infinite; this corresponds to ballistic propagation. If width grows with the square root of time, a finite diffusivity is obtained; this corresponds to diffusive propagation. A third possibility exists, namely that the width of the wave-packet saturates to a constant value over which the vibration is localized [48]. Such localized modes, typically occur at high ω [41]. The diffusivity is vanishingly small and $d(\omega)$ cannot be factorized into the product of $\ell(\omega)$ and v, as in Eq. (5), because no speed of sound can be associated with such vibrational modes.

In this study, we calculate the diffusivity by evaluating the Kubo formula for $d(\omega)$ directly [5] for computer-generated packings in terms of the normal modes over the entire frequency range available. The rationale behind this choice is twofold. On one hand, we use the energy diffusivity as a spectral measure of transport to probe the character of the vibrational normal modes of a jammed solid. On the other

hand, we use the jammed solid as a model amorphous structure whose transport properties can be studied as a function of pressure simply by varying the density relative to that of the unjamming transition. This allows variation over orders of magnitude of pressure, which cannot be realized in more realistic models of molecular or network glasses.

A. Review of the Kubo formula for the energy diffusivity

The analogy between the thermal conductivity in the phononic problem and its better studied electrical counterpart underlies many of the mathematical techniques and physical concepts employed in our investigation.

The Kubo formula for the energy diffusivity was derived in a convenient form by Allen and Feldman in Ref. [5]. Consider the *volume-averaged* energy current S that arises in response to an applied thermal gradient ∇T. In linear response, S is given by

$$S = -\kappa \nabla T, \tag{13}$$

where κ is the thermal conductivity. More generally, the ac thermal conductivity $\kappa_{\mu\nu}(T,\Omega)$, which relates the energy flux S_μ in the μ direction to the time-varying temperature gradient in the ν direction, $\partial_\nu T \; e^{i\Omega t}$, is

$$\kappa_{\mu\nu}(T,\Omega) = \frac{1}{VT}\int_0^\beta d\lambda \int_0^\infty dt e^{i(\Omega+i\eta)t}\langle S_\mu(-i\hbar\lambda)S_\nu(t)\rangle, \tag{14}$$

where V is the volume of the system and the angular brackets denote an equilibrium average of the autocorrelation function of the energy current operator $\hat{S}$.

[Note that Eq. (14) is analogous to the Einstein relation for the diffusion coefficient of an ensemble of Brownian particles in terms of the velocity-autocorrelation function. The main difference lies in the fact that in the thermal problem the conserved quantity is the energy density $\hat{h}$ that obeys the continuity equation:

$$\frac{\partial \hat{h}}{\partial t} = -\vec{\nabla}\cdot\vec{s}(r), \tag{15}$$

where $s(r)$ is the local energy-flux operator (assumed to be isotropic for simplicity) prior to the spatial average that leads to $\hat{S}$. In the case of the Einstein relation, the conserved quantity is the particle number and the role of $s(r)$ is played by the particle current.]

Our aim is to extract an expression for the diffusivity $d(\omega)$ by comparing Eq. (14) to Eq. (4) when the dc limit of $\kappa(T,\Omega)$ is taken, that is, when $\Omega \to 0$. We first recast Eq. (14) in terms of a discrete sum over modes i:

$$\kappa_{\mu\nu}(T,\Omega) = \frac{1}{VT}\sum_{ij}\frac{n_j-n_i}{\hbar(\omega_i-\omega_j)}(S_\mu)_{ij}(S_\nu)_{ji}\delta(\omega_i-\omega_j-\Omega), \tag{16}$$

where n_i is the equilibrium occupation number for bosons $n_i=[\exp(\beta\hbar\omega_i)-1]^{-1}$ and $(S_\mu)_{ij}$ is the matrix element of the energy-flux operator in the μ direction. This matrix element

can be computed from the vibrational normal modes, which are obtained from the dynamical matrix, $H^{mn}_{\alpha\beta}$, whose i^{th} normalized eigenvector is denoted by $e_i(m;\alpha)$, where $\{m,n\}$ and $\{\alpha,\beta\}$ label particles and their Cartesian coordinates, respectively [49]. For disordered solids, the modes must be determined by numerical diagonalization of the dynamic matrix.

In an isotropic system a scalar thermal conductivity $\kappa(T)$ can be meaningfully defined from the trace of the tensor $\kappa_{\mu\nu}(T)$

$$\kappa(T) = \frac{1}{3}(\kappa_{xx}+\kappa_{yy}+\kappa_{zz}), \tag{17}$$

To simplify Eq. (16) further, consider that in the limit $\Omega \to 0$ the delta function forces the factor $(n_j-n_i)/(\omega_i-\omega_j)$ to become $-\partial n_i/\partial\omega_i$. One can then use Eq. (17) in conjunction with the identity

$$C(\omega_i,T) = -\left(\frac{\hbar^2\omega_i^2}{VT}\right)\left(\frac{\partial n_i}{\partial\omega_i}\right) = k_B(\beta\hbar\omega_i)^2\frac{e^{\beta\hbar\omega_i}}{(e^{\beta\hbar\omega_i}-1)^2}, \tag{18}$$

to show that the thermal conductivity of Eq. (16) can indeed be factorized as indicated in Eq. (2) with $d(\omega_i)$ given by [5]

$$d(\omega_i) \equiv \frac{\pi}{3}\sum_j (\hbar\omega_i)^{-2}|\vec{S}_{ij}|^2\delta(\omega_i-\omega_j), \tag{19}$$

where the matrix elements $\vec{S}_{ij}$ read [5]

$$\vec{S}_{ij} = \frac{(\omega_i+\omega_j)^2}{4\omega_i\omega_j}\sum_{mn,\alpha\beta}(\vec{r}_m-\vec{r}_n)e_i(m;\alpha)H^{mn}_{\alpha\beta}e_j(n;\beta). \tag{20}$$

In the limit $\omega_i \to \omega_j$ enforced by the delta function in Eq. (19), the prefactor $\frac{(\omega_i+\omega_j)^2}{4\omega_i\omega_j} \to 1$. However, taking this limit requires special care when the Kubo formula (derived in the continuum limit) is evaluated for a finite and isolated system with a discrete spectrum [50]. Inspection of Eq. (20) reveals that the diagonal matrix elements S_{ii} vanish. On the other hand any contribution to $d(\omega_i)$ coming from the nondiagonal matrix elements S_{ij} with $i \neq j$ is given zero weight when the delta function $\delta(\omega_i-\omega_j)$ is strictly enforced. This difficulty can be circumvented by smoothing out the δ functions in Eq. (19) with the small finite width η

$$\delta_\eta(\omega_i-\omega_j) = \frac{\eta}{\pi[(\omega_i-\omega_j)^2+\eta^2]}. \tag{21}$$

This heuristic procedure is expected to give the correct "bulk" result as long as the broadening η is (a) much larger than the average level spacing, Δ, and (b) much smaller than any characteristic frequency scale relevant to the problem. In this paper, the broadening of the delta function η in Eq. (21) is typically chosen to be approximately five times larger than the average level spacing, Δ. We have verified that our numerical results do not depend on this choice as long as conditions (a) and (b) are met. In the Landauer formulation of transport, it is not necessary to introduce the level broadening η by hand because the inherent coupling of the system to the reservoirs plays an analogous role [51].

One advantage of studying the energy diffusivity instead of the thermal conductivity is that $d(\omega)$ is finite at nonzero frequency when evaluated at the harmonic level. By contrast, $\kappa(T)$ is generally infinite if anharmonic corrections are ignored. This is because $d(\omega)$ in the integrand of Eq. (4) diverges too strongly at low ω due to phonons that are progressively less scattered with increasing wavelength.

One main result of this paper will be that a marginally jammed solid is an exception to the rule that the thermal conductivity should diverge within the harmonic approximation. However, as the system is compressed above point J, $\kappa(T)$ again diverges, as in the standard case.

In order to cure this divergence, additional scattering mechanisms, beyond harmonic theory, are typically invoked resulting in an additional contribution to the diffusivity, $d_c(\omega)$. Upon adding $d_c(\omega)$ to the harmonic contribution, $d(\omega)$, (for example, as if they were two conductors in series [52]), one obtains the total diffusivity $d_T(\omega)$,

$$d_T(\omega)^{-1} = d(\omega)^{-1} + d_c(\omega)^{-1}, \qquad (22)$$

Graebner, Golding, and Allen have demonstrated that the thermal conductivity of many glassy materials can be fitted by assuming an expression for $d_T(\omega)$ consistent with Eq. (22) or more accurately its analog in terms of the mean-free-path $\ell(\omega)$ [53]. According to their analysis, the first contribution in Eq. (22), $d(\omega)$, corresponds to a mean free path that exhibits a cross-over from Rayleigh law $\ell(\omega) = \omega^{-4}$ to a frequency-independent value ℓ_{min}. The second low ω contribution, $d_c(\omega)$, arises from assuming resonant scattering and relaxational absorption of propagating phonons by two-level systems [11].

In this study we do not attempt to guess $d_c(\omega)$, instead we determine how the *harmonic* scattering mechanisms assumed in Ref. [53] depend on applied pressure and the choice of interparticle potential in a model amorphous solid formed by densification of soft spheres. It is instructive to compare the result of our harmonic calculations of $d(\omega)$ summarized in Figs. 1 and 2, to the mean free path represented in Fig. 3 of Ref. [53] which incorporates the low ω anharmonic corrections.

Since the Kubo formalism does not rely on the assumption of propagating phonons we expect our results for $d(\omega)$ to be valid even in the high-frequency regime, where the diffusivity cannot be factorized into a product of $\ell(\omega)$ times a frequency-independent speed of sound. This spectral regime of the diffusivity is essential to capture the upturn in the thermal conductivity which occurs above the plateau. While, the cutoff contribution $d_c(\omega)$ necessarily dominates at low temperature, much progress can be made in understanding the plateau in the thermal conductivity and the subsequent rise by studying the harmonic contribution, which dominates as T increases.

B. Model

Our simulations are carried out on jammed sphere packings, as described in Sec. II B. Specifically, we study a 50/50 bidisperse mixture comprised of $250 \le N \le 10\,000$ frictionless spheres with a diameter ratio of 1.4, interacting with
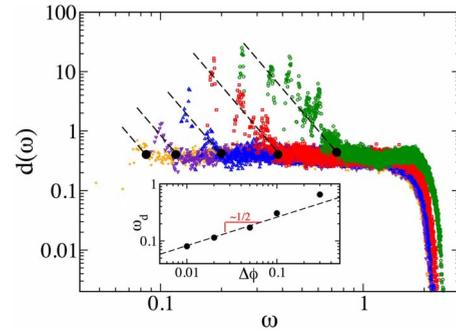

FIG. 1. (Color online) Plots of diffusivity, measured in units of $\sigma\sqrt{\epsilon/M}$ versus frequency, measured in units of $\sqrt{\epsilon/\sigma^2 M}$ for an unstressed packing of 2000 particles with harmonic interactions at packing fractions $\Delta\phi = 0.3$ (green circles), 0.1 (red squares), 0.05 (blue upside triangles), 0.02 (purple downside triangles), and 0.01 (yellow crosses). The black dots indicate the crossover frequency ω_d at each $\Delta\phi$, while the dashed lines show a power law of ω^{-4}, expected for weakly scattered plane waves. The plateau diffusivity is $d_0 \approx 0.35$. The inset shows the packing fraction scaling of ω_d.

potentials described in Eq. (6) with $\alpha = 2$ and $\alpha = 5/2$. The packing fraction at the onset of jamming, ϕ_c, is characterized by the onset of a nonzero pressure. We determine ϕ_c and obtain $T = 0$ configurations at controlled $\Delta\phi \equiv \phi - \phi_c$ as in Ref. [14]. For each configuration, we diagonalize its dynamical matrix and find the eigenvectors and the corresponding eigenfrequencies, which are measured in units of $\sqrt{\epsilon/M\sigma^2}$, where M is the particle mass [14]. Rattler particles with less than three contacts are unstable and they have been removed
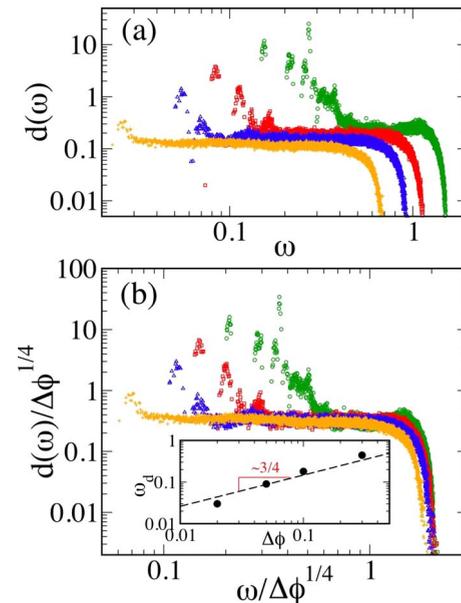

FIG. 2. (Color online) Plots of diffusivity vs frequency for an unstressed packing of 2000 particles interacting via a Hertzian potential. The packing fractions are approximately $\Delta\phi = 0.3$ (green circle), 0.1 (red squares), 0.05 (blue triangles), and 0.02 (yellow crosses). (a) $d(\omega)$ in units of $\sigma\sqrt{\frac{\epsilon}{M}}$ vs ω (in units of $\sqrt{\frac{\epsilon}{\sigma^2 M}}$), (b) scaled diffusivity, $d(\omega)/\Delta\phi^{1/4}$, vs scaled frequency, $\omega/\Delta\phi^{1/4}$, showing data collapse in the plateau region. The inset shows the packing fraction scaling of the crossover frequency ω_d.

before performing the normal mode analysis.

We primarily consider an "unstressed" version of this model [54], which is particularly tractable. We use energy-minimized configurations obtained from numerically generated jammed sphere packings as described above. We then replace the interaction potential, $V(r_{ij})$, between each pair of overlapping particles with an unstretched spring with the same stiffness, $V''(r_{ij}^{eq})$, where r_{ij}^{eq} is the equilibrium distance between particles i and j. Note that since r_{ij}^{eq} takes a different value between distinct particle pairs there will be a distribution in the local values of the elastic constants. On the other hand, the fact that all springs are unstretched guarantees that there are no net forces between particles in their equilibrium positions so that stable configurations for the stressed system are also stable in the unstressed one.

The unstressed packings correspond to dropping terms depending on the first spatial derivative of the potential, V', in the dynamical matrix obtained from expanding the energy around the equilibrium position of the particles,

$$\delta E = \frac{1}{2} \sum_{n,m} \left[V''(r_{nm})(\delta \vec{R}_{nm} \cdot \hat{r}_{nm})^2 + \frac{V'(r_{nm})}{r_{nm}}(\delta \vec{R}_{nm}^{\perp})^2 \right].$$

(23)

where n, m are indexes labeling the particles.

The approximation of dropping the V' stress term in Eq. (23) generates an interesting disordered system in its own right. The resulting off-lattice model, comprised of point particles interacting with relaxed springs, exhibits both spatial fluctuations in the local elastic stiffness as well as topological disorder (e.g., fluctuations in the local coordination number). Moreover, its amorphous structure can be varied by changing the volume.

The effect of the stress term can be seen from Eq. (23). Since V' is negative for repulsive interactions, the stress term lowers δE and hence the mode frequency. We will discuss the effect of the stress term on the diffusivity of a jammed solid in Sec. V C.

IV. ENERGY TRANSPORT CROSSOVER IN MODEL JAMMED SOLIDS

Figure 1 shows a scatter plot of the mode diffusivity $d(\omega_i)$ obtained from evaluating numerically Eq. (19) and (20) at five packing fractions $\Delta\phi = 0.3$ (green circles), 0.1 (red squares), 0.05 (blue upside triangles), 0.02 (purple downside triangles), and 0.01 (yellow crosses) for a 2000-particle packing. Three distinct transport regimes can be clearly identified in each curve, corresponding to weakly scattered, diffusive, and localized vibrational modes. The characteristic frequencies that mark the crossover between the plateau in $d(\omega)$ and the diverging low ω branch are indicated in Fig. 1 as black dots and do not depend on N for systems of this size or larger. In what follows, the mode diffusivity data is presented as scatter plots of single particle configurations for clarity. We have tested that performing a frequency binning followed by a disorder average over several distinct configurations confirms our conclusions [15].

At very high frequencies, the diffusivity drops rapidly as a result of localization of the vibrational modes. The contribu-

tion of localized modes to the thermal conductivity is negligible if anharmonic effects such as hopping are ignored. Figure 1 shows that the localization frequency for particles interacting with a repulsive harmonic potential does not depend strongly on $\Delta\phi$ close to the jamming point.

At low frequencies, the energy diffusivity exhibits a strong frequency dependence characteristic of vibrational modes that are essentially phonons weakly scattered by disorder. As a comparison we have drawn black dashed lines in Fig. 1 indicating the power-law divergence with ω^{-4} expected for Rayleigh scattering of plane waves incident on uncorrelated scattering centers. Close inspection of the scatter plot reveals that the low ω peaks occur close to the discrete frequencies allowed in our cubic simulation box of size L by the linear dispersion [55,56],

$$\omega_i = \frac{2\pi v_t}{L}\sqrt{p^2 + q^2 + r^2},$$

(24)

where $\{p,q,r\}$ denote the quantum numbers for the periodic system and the speed of sound v_t is the transverse one for most low ω modes near ϕ_c, see Eq. (10) and (11). In the continuum limit we expect that their density of states at very low ω will be given by the Deybe law $D(\omega) \sim \frac{\omega^2}{v^3}$.

The intermediate frequency regime is the one of most direct relevance to the intermediate temperature behavior of the thermal conductivity. Strikingly, this regime is characterized by a diffusivity, henceforth labeled as d_0, that is nearly independent of frequency (Fig. 1). The notion of a frequency-dependent diffusivity has a long history dating back to Kittel's observation [40] that the experimental curve for $\kappa(T)$ in many glasses at room temperature could be interpreted in terms of a nearly frequency-independent mean free path of the order of a molecular length.

The onset of the plateau in the diffusivity is marked by a crossover frequency, that exhibits a peculiar scaling with the packing fraction $\Delta\phi$. We henceforth label it as ω_d. The inset of Fig. 1 reveals that $\omega_d \sim \Delta\phi^{0.5}$ for a system composed of harmonic springs. This is the same scaling with $\Delta\phi$ observed for the frequency ω^* above which a large excess of vibrational modes have been observed in previous studies of the density of states [see Eq. (12) with $\alpha=2$].

A. Dimensional analysis

Figure 1 shows that $d(\omega)$ is characterized by a well-defined crossover from ballistic to diffusive behavior. Our aim in this section is not to provide a rigorous derivation of the functional dependence of the diffusivity on frequency, but rather to understand how the defining features of the diffusivity (the height of the plateau, d_0, and the scaling of the crossover frequency, ω_d) depend on applied pressure. This is done by keeping track of how the fundamental parameters that enter the definition of $d(\omega)$ scale with the packing fraction $\Delta\phi$. First, however, we must understand how these parameters depend on the dimensional parameters in our system: the particle diameter, σ, the particle mass, m, and the energy scale for the potential, ϵ.

The diffusivity has dimensions of $\frac{[\text{length}]^2}{\text{time}}$. The natural unit of frequency in a vibrational system, by which the ω axis in

Fig. 1 is measured, is $\sqrt{\frac{k}{M}}$ where k is the *bare* elastic coupling of the solid. More generally an effective spring constant, k_{eff}, can be defined by differentiating twice the interaction energy $V(r_{ij})$ of Eq. (6) and evaluating the result at the average equilibrium bond length $\langle r_{ij}^{eq} \rangle$ of interacting neighbors,

$$k_{eff} = \left. \frac{\partial^2 V(r_{nm})}{\partial r_{nm}^2} \right|_{r_{nm} = \langle r_{nm}^{eq} \rangle}. \tag{25}$$

There is a simple linear relation between the relative change in $\langle r_{nm}^{eq} \rangle$ upon compression and the corresponding macroscopic change in volume $\Delta \phi$,

$$\frac{\sigma - \langle r_{nm}^{eq} \rangle}{\sigma} \approx \frac{\Delta \phi}{3}, \tag{26}$$

where the numerical prefactor in the right-hand side of Eq. (26) was checked numerically [57].

From Eqs. (25) and (26) we see that

$$k_{eff} \approx \epsilon \frac{\alpha - 1}{\sigma^2} \left(\frac{\Delta \phi}{3} \right)^{\alpha - 2}, \tag{27}$$

For harmonic repulsions, $\alpha = 2$ and $k_{eff} = \epsilon / \sigma^2$ is independent of $\Delta \phi$, while for Hertzian potentials, $k_{eff} \sim \Delta \phi^{1/2}$.

Note that the bulk modulus obeys the same scaling [13,45], so

$$B \sim k_{eff}, \tag{28}$$

whereas according to Eqs. (7) and (8) the shear modulus scales as

$$\frac{G}{k_{eff}} \sim \Delta z \sim \Delta \phi^{1/2}, \tag{29}$$

independent of α. The difference in the scaling properties of the bulk and shear modulus upon compression is the hallmark of the anomalous elasticity of jammed solids whose consequence for energy transport will be explored in the next section.

The dimensional length scale in this problem is the particle size, σ. As a result, the diffusivity is naturally measured in units of the product of σ^2 times the characteristic frequency scale

$$d(\omega) \sim \sigma^2 \sqrt{\frac{k_{eff}}{M}}. \tag{30}$$

Inspection of Fig. 1 reveals that, as ω increases, the diffusivity decreases rapidly until it saturates at a value that we denote by d_0. Note from Fig. 1 that $d_0 \approx 0.35 \sigma^2 \sqrt{k_{eff}/M}$ $= 0.35 \sigma \sqrt{\epsilon/M}$, see Eq. (30).

Similarly, upon evaluating Eqs. (27) and (30) for a Hertzian potential ($\alpha = 5/2$) in three dimensions, we obtain the following prediction for the value of d_0

$$d_0 = c \frac{3^{1/4}}{2^{1/2}} \sigma \sqrt{\frac{\epsilon}{M}} \Delta \phi^{1/4} \quad \text{Hertzian.} \tag{31}$$

$d_0 = c \sigma \sqrt{\epsilon/M} \Delta \phi^{1/4}$ where c is of order unity. Figure 2(a) shows $d(\omega)$ for a Hertzian system at four different packing

fractions. Clearly, d_0 increases with $\Delta \phi$. If we divide $d(\omega)$ and ω by $\Delta \phi^{1/4}$ as in Fig. 2(b) we get a good collapse of the data, indicating that d_0 obeys the prediction, with $c = 0.35$. The numerical value of c is independent of the potential used and will be derived purely from the random geometry of a marginally jammed packing in Sec. V B.

We note that the application of the Kubo formula to the Hertzian packings rests on the observation that the energy of a particle slightly displaced from its equilibrium position is harmonic even if the interparticle interaction is not a quadratic function of the particle overlap. The validity of the linear response theory adopted in this work can be independently tested by performing direct molecular dynamics simulations of the energy diffusivity [4,5] and the thermal conductivity [58].

These results for harmonic and Hertzian potentials suggest that the plateau in the diffusivity is consistent with what is loosely referred to as the "minimal conductivity hypothesis" [40,59]. The diffusivity d_0 is minimal in the sense that the length scale that multiplies the characteristic frequency is the smallest length that can be chosen in the system, the particle diameter σ.

Once $d(\omega)$ attains its "minimal" value it cannot decrease by much as ω increases, unless a transition occurs to a new transport regime characterized by a vanishingly small diffusivity. This is precisely what happens at the end of the plateau where localization sets in.

B. Scaling of transport crossover

In this section, we provide a scaling argument for the dependence of the crossover frequency ω_d. At the crossover, where the diffusivity plateau d_0 begins and the regime of diverging diffusivity has just ended, the kinetic formula for the diffusivity, Eq. (5) leads

$$d_0 = \frac{1}{3} v_t \, \ell_d. \tag{32}$$

In writing Eq. (32), we have assumed that an effective transverse speed of sound can be assigned to the vibrational modes at the onset of the plateau. This working assumption is corroborated in Sec. IV D where the dispersion relation determined numerically is found to be approximately linear up to the crossover frequency ω_d and to exhibit a smooth crossover above it. The transverse speed of sound is chosen because the phonon density of states at low ω is dominated by shear waves near point J as apparent from Eqs. (10) and (11) and the discussion following it.

We can now solve Eq. (32) for the mean-free path ℓ_d at the crossover

$$\ell_d = \frac{3 d_0}{v_t} \sim \sqrt{\frac{k_{eff}}{G}}, \tag{33}$$

where we used the expression for d_0 given in Eq. (30) and the fact that the transverse sound speed v_t is proportional to the square root of the shear modulus G.

Upon substituting Eq. (29) into Eq. (33), one obtains an expression for the packing fraction dependence of ℓ_d which is independent of α

$$\ell_d \sim \Delta z^{-1/2} \sim \Delta\phi^{-1/4}. \qquad (34)$$

Upon approaching point *J*, the mean free path ℓ_d at the onset of the diffusivity plateau becomes arbitrary large compared to the particle size σ. The scaling in Eq. (34) is consistent with previous numerical studies of the peak position (as a function of wavevector) of the *transverse* structure factor measured at the frequency onset of excess modes, which found a scaling of $\Delta\phi^{0.24\pm0.03}$ [14].

It is instructive to compare ℓ_d to a second characteristic length present in this problem, namely, the ratio between the transverse speed of sound and the crossover frequency ω_d. More precisely we wish to compare ℓ_d to $1/q_d$, the wavelength of the transverse wave that would exist in the spectrum of an ordered solid according to the dispersion relation $\omega_d = v_t q_d$. We find that over our range of compression

$$q_d \, \ell_d \sim 2. \qquad (35)$$

That is to say, the wavelength $1/q_d$ is of order of the mean-free path ℓ_d at the onset of the diffusivity plateau, independently of the packing fraction.

Upon substituting Eq. (34) in the dispersion relation and using Eqs. (27) and (8), we obtain

$$\omega_d \sim \frac{v_t^2}{k_{eff}} \sim \frac{G}{\sqrt{k_e ff}} \sim \Delta\phi^{(\alpha-1)/2}. \qquad (36)$$

It is straightforward to conclude from Eq. (36) that ω_d should scale as $\Delta\phi^{1/2}$ and $\Delta\phi^{3/4}$ for harmonic and hertzian interactions, respectively. This conclusion is consistent with the numerical results plotted in the insets of Figs. 1 and 2(b).

Indeed when ω_d is measured in the natural dimensionless units of $\sqrt{\frac{k_{eff}}{M}}$, as in Fig. 2, it is simply given by ratio of the shear modulus and the effective spring constant. Upon substituting Eq. (29) into Eq. (36), one obtains

$$\frac{\omega_d}{\sqrt{k_{eff}}} \sim \frac{G}{k_{eff}} \sim \Delta z \sim \Delta\phi^{1/2}, \qquad (37)$$

independently of α. The scaling analysis leading to Eqs. (34) and (37) suggests that the scaling of ℓ_d and ω_d can be traced to the anomalous scaling of the shear modulus in the vicinity of the unjamming transition.

The argument presented above does not assume that the mean-free path is necessarily comparable to the wavelength, as ω_d is approached from below. See for example the calculations performed on the mean-field model of Ref. [60] where this is not the case. In future work, we hope to probe with greater spectral resolution the behavior of the diffusivity in the crossover region for a larger range of packing fraction to conclusively settle these issues. The limited dynamic range attained in the simulations presented in this study stems from the fact that the crossover cannot be seen if ℓ_d exceeds the system size. The disappearance of the low-ω diffusivity upturn at the lowest $\Delta\phi$ is clearly seen in Figs. 1 and 2, indicating that for smaller values of the packing fraction the system size used in the simulation is not large enough to study the transport crossover.
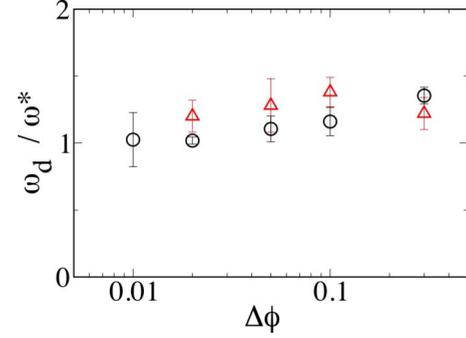

FIG. 3. (Color online) Plot of the transport crossover versus the boson peak at different $\Delta\phi$ in jammed packings of 2000 particles with harmonic (black open circles) and Hertzian (red open triangles) repulsions. The ratio is near unity and is nearly constant with $\Delta\phi$.

C. Relation of transport crossover to boson peak

In this section we show numerically that the transport crossover frequency ω_d observed in the diffusivity plots of Figs. 1 and 2, corresponds to the same frequency scale, ω^*, at which the onset of the excess vibrational modes is observed in the density of states. The advantage of jammed sphere packings over models studied previously is that one can verify this identification at different packing fractions and hence test not only that the two frequency scales are close in numerical value for a given ϕ but also that they scale in the same way as a function of compression.

We first note that the scaling for ω_d in Eq. (36) is identical with the earlier numerical observation of the boson peak frequency, ω^*, in Eq. (12) as well as with the relation derived theoretically in Ref. [23] for the frequency onset of the anomalous modes of compressed jammed packings. Figure 3 shows the ratio ω_d/ω^* as a function of compression, $\Delta\phi$. Here, the frequency ω^* is measured numerically from the onset of the plateau in the density of states; see Ref. [61] for details. The variation of the ratio ω_d/ω^* is small compared with the variation of ω_d, which changes by an order of magnitude over the same range of $\Delta\phi$ (see inset to Fig. 1). Thus, the transport crossover frequency and boson peak frequency track each other, implying that the same physics underlies both phenomena. In particular, the result shows that the excess modes above the boson peak frequency have a small and nearly frequency-independent diffusivity.

D. Change in nature of modes at transport crossover

The Fourier decomposition of the vibrational modes evolves dramatically as the frequency is increased through the transport crossover at ω_d. We concentrate here on $f_T(q,\omega)$, the transverse Fourier components [62,63]:

$$f_T(q,\omega) = \left\langle \left| \sum_n \hat{\mathbf{q}} \wedge \mathbf{e}_n(\omega) \exp(\iota\mathbf{q} \cdot \mathbf{r}_n) \right|^2 \right\rangle, \qquad (38)$$

where *q* denotes the wave vector and $\mathbf{e}_n(\omega)$ is the polarization vector of particle *n* of the mode at frequency, ω. The brackets indicate an average over directions of $\hat{q}$.

At all compressions, $f_T(q,\omega)$ has a low-wave-vector peak at $q=q_{max}$ that shifts to higher values with increasing fre-
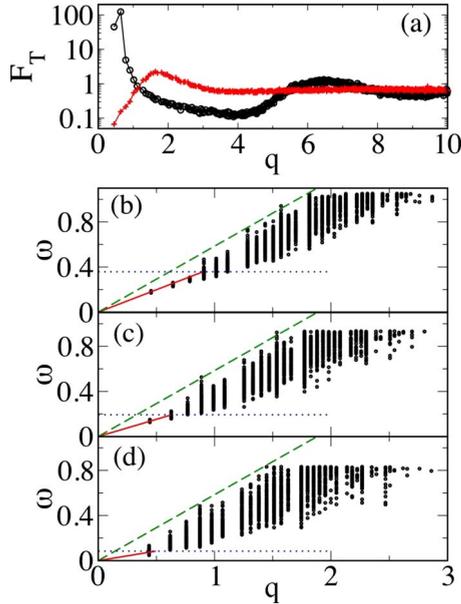
FIG. 4. (Color online) Transverse mode structure factor $f_T(q, \omega)$ for $N = 2000$ and $\Delta\phi = 0.1$ at $\omega = 0.23$ (black circles) below the transport crossover at $\omega_d = 0.36$ and at $\omega = 0.74$ (red crosses) well above the crossover. (b)–(d) Phonon dispersion relations for (b) $\Delta\phi = 0.1$, (c) 0.05, and (d) 0.01, respectively. The data are at discrete values of q because of the finite system size. The horizontal (blue) dotted line in each panel (b)–(d) marks ω_d, while the solid (red) line marks the transverse sound speed that varies with compression as given by Eq. (10). As a comparison, the dashed (green) line is the same in each panel (independent of compression) and has a slope proportional to the speed of longitudinal sound. Note that the solid line gives the dispersion for frequencies below ω_d.

quency. Two typical examples are shown in Fig. 4(a) at $\Delta\phi = 0.1$. Well below ω_d (black dots), where the diffusivity decreases rapidly with increasing frequency, the peak is sharp and tall. Here the modes resemble weakly scattered transverse plane waves with wave vector q_{max}. By contrast well above ω_d (red crosses), in the region of the diffusivity plateau, the peak is dramatically less pronounced; the peak height is ~50 times smaller than for the black curve and is comparable to the background signal observed at higher q. This is the characteristic signature of the strong-scattering regime where vibrational modes can no longer be meaningfully characterized by a narrow range of q. Such modes are poor conductors of energy, as reflected in the low value of $d(\omega)$ above ω_d. This evolution in character is not sharp and the peak height decreases continuously as ω increases past ω_d; a peak—albeit a small one—appears even for modes in the diffusivity plateau.

From data of q_{max} versus ω one can determine the transverse-sound dispersion curve [62,63]. Figures 4(b)–4(d) shows the transverse dispersion relation for three of the packing fractions shown in the diffusivity plot of Fig. 1. Each point represents the value of q_{max} obtained from the peak in $f_T(q, \omega)$ for a single vibrational mode of frequency ω. In other words, each point represents the wavevector that makes the largest contribution to a vibrational mode. At each packing fraction the crossover frequency ω_d is represented

by a horizontal dotted line. The solid red line, $\omega = v_t q$, shows the expected transverse dispersion relation with v_T decreasing with decreasing $\Delta\phi$ on the basis of Eq. (10). The dashed green line in each panel has the same slope independent of $\Delta\phi$. From Eq. (10), its slope is therefore proportional to (but smaller than) the longitudinal sound speed, v_l.

These dispersion curves also show a marked change in behavior as the frequency is varied through ω_d. Well below the crossover frequency, the peaks are not only sharp, as indicated by the behavior in Fig. 4(a), but their position corresponds with that given by the transverse speed of sound (red solid line) [55,56]. As ω increases above ω_d, the peaks broaden and they start to depart from the line given by the transverse sound speed. Instead, the lowest values of q_{max} shift to smaller q and begin to track the green line which has a slope independent of compression and proportional to the longitudinal, not the transverse, speed of sound. The spread in the positions of q_{max} for frequencies $\omega > \omega_d$ indicate that the peaks are very broad in this region. Similar results for $f_T(q, \omega)$ and the transverse dispersion relation above ω_d were earlier found for a model that included the stress terms in the energy [63]. In that case, the dispersion relation above ω_d, showed essentially no variation in the position of the peaks, q_{max}, despite an increase in $\Delta\phi$ by five orders of magnitude. [The data in that study is slightly different from the data reported here in that it showed averaged $f_T(q, \omega)$ over several nearby frequency modes in a bin instead of the peaks in individual modes. Both ways of treating the data show the same general features.]

V. PLATEAU IN THE DIFFUSIVITY

In the previous section, we have shown that ω_d, where the diffusivity flattens out, scales in the same way as does the frequency associated with the excess modes in the density of states. We can thus consider the flat diffusivity as the transport signature of the excess vibrational modes that generate the boson peak. In the present section, we will focus on why the diffusivity is flat over an extended frequency range above ω_d. We will address this (A) by showing that from the form of the matrix elements, the diffusivity should be simply proportional to the density of the modes themselves, which is also flat in this region, and (B) by examining what properties of the modes are necessary for producing a flat diffusivity. Our study suggests that $\omega_d \sim \omega^*$ vanishes at point J. At this point, the plateau extends over the entire frequency range up to the onset of localization. This simplifies the analysis. Thus, Point J is a natural place to gain insight into the origin of the constant diffusivity.

A. Energy-flux matrix elements

We start by showing that the energy-flux matrix elements have a particularly simple form at the jamming threshold, which enables us to determine the $N \to \infty$ behavior of the diffusivity [15]. Consider the frequency averaged matrix elements defined as

$$|\vec{\Sigma}(\omega, \omega')|^2 = \sum_{ij} |\vec{S}_{ij}|^2 \delta(\omega - \omega_i) \delta(\omega' - \omega_j), \quad (39)$$

where i and j are indexes labeling the vibrational modes and the matrix elements $\vec{S}_{ij}$ are given by Eq. (20) in the limit $\omega_i \to \omega_j$.
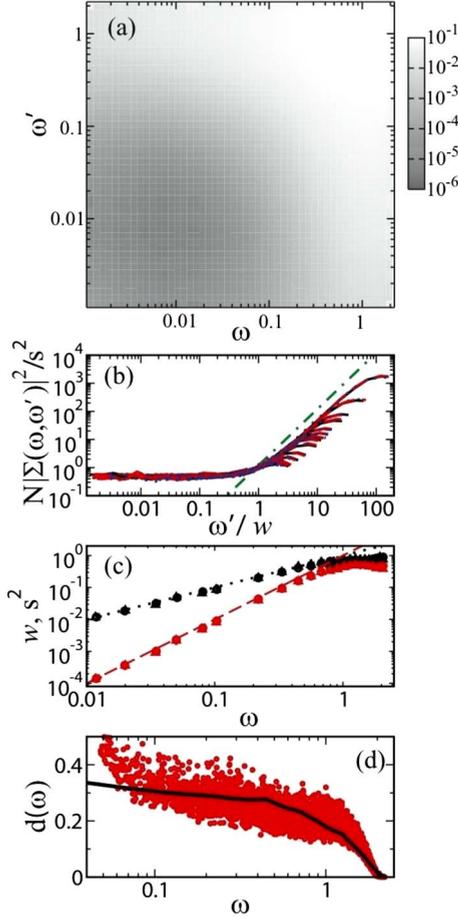
FIG. 5. (Color online) Diffusivity just above the jamming transition at $\Delta\phi=10^{-6}$. (a) Contour plot of the heat-flux matrix elements $|\Sigma(\omega,\omega')|^2$ plotted versus ω and ω' at $N=2000$. (b) Scaling plot showing collapse of $|\Sigma(\omega,\omega')|^2$ at $N=2000$ (black solid), 1000 (red dashed), and 500 (blue dotted) with scale factors s^2 and w. (c) Scale factors s^2 (red symbols), and w (black symbols) versus ω. We find $s^2 \propto \omega^2$ (red dashed line) and $w \propto \omega$ (black dotted line) except at high ω. (d) Scatter plot of $d(\omega)$ with $N=2000$ and delta function broadening $\eta=0.002$. Solid line shows the predicted $d(\omega)$ for the infinite system.

Figure 5(a) shows the heat-flux matrix elements $|\vec{\Sigma}(\omega,\omega')|^2$ defined in Eq. (39) for packings at $\phi-\phi_c=10^{-6}$ for different values of ω versus ω'. Note that the matrix elements are symmetric in ω and ω' and that they increase with increasing ω and ω'. Figure 5(b) shows that all the curves for different system sizes, N, and frequencies, ω, can be collapsed onto a simple scaling form given by

$$|\vec{\Sigma}(\omega,\omega')|^2 \sim \frac{1}{N}\omega'^2 \quad \text{if } \omega' > \omega,$$

$$|\vec{\Sigma}(\omega,\omega')|^2 \sim \frac{1}{N}\omega^2 \quad \text{if } \omega' < \omega, \qquad (40)$$

except at high frequency where the modes become localized [63–66] and the curves in Fig. 5(b) start peeling off from the dashed-dotted (green) line. Figure 5(c) shows that the scale

factors for the collapse satisfy $s^2=\omega^2$ and $w=\omega$, respectively, consistently with Eq. (40). The scaling collapse demonstrates that the only noticeable system-size dependence is a prefactor of $1/N$ [67]. Since for large N, the density of states scales as N [14], Eq. (4) therefore yields a well-defined diffusivity in the $N\to\infty$ limit, shown as the solid curve in Fig. 5(d).

The scaling collapse in Fig. 5(b) implies that $|\vec{\Sigma}(\omega,\omega)|^2 \propto \omega^2/N$ at low frequencies. This result, combined with Eq. (19), implies that $d(\omega) \propto D(\omega)$ at low ω. This $N\to\infty$ prediction for $d(\omega)$ is shown as the solid line in Fig. 5(d). Thus, the diffusivity is nearly constant down to $\omega=0$ at point J because the density of states is nearly constant there [14].

Over most of the frequency range, this $N\to\infty$ prediction agrees very well with the scattered points in Fig. 5(d), which show $d(\omega)$ for a system with $N=2000$. At low frequency $d(\omega)$ deviates from the solid line and exhibits an upturn. This upturn is a finite-size artifact that arises from replacing the delta function with a smoothing function in Eq. (21). It scales as ω^{-3} with a prefactor that vanishes as $N\to\infty$ and $\eta\to0$.

B. Properties of modes in the plateau

It is important to understand what specific properties of the modes give rise to the plateau in the diffusivity. To simplify the analysis, we will consider only systems of monodisperse particles interacting via harmonic repulsions ($\alpha=2$) just above the jamming threshold. The argument can be generalized to the bidisperse case studied in this paper.

The starting point for deriving the flat diffusivity and for deriving its plateau value, d_0, is Eq. (20) for the matrix element of the heat-flux operator evaluated using periodic boundary conditions. Recall that for two modes of frequencies within a bin centered at ω the matrix element S_{ij} reads

$$S_{ij} = \frac{hi}{2VM}\sum_{n,m} \vec{e}(n,i)H(\vec{R}_m,\vec{R}_n)\vec{e}(m,j)(\vec{R}_m-\vec{R}_n), \quad (41)$$

where n and m label the particles, $\vec{R}_n$ and $\vec{R}_m$ their positions, $H(\vec{R}_m,\vec{R}_n)$ is the dynamical matrix element (itself a $\mathcal{D}*\mathcal{D}$ matrix in $\mathcal{D}$ dimensions) between these two particles, $\vec{e}(n,i)$ is the displacement of particle n in mode i and M is the particle mass. (Note that Eq. (41) differs slightly in notation from Eq. (20) because the latter indicates the Greek indexes corresponding to Cartesian coordinates explicitly.)

Next set $(\vec{R}_m-\vec{R}_n)=\sigma\hat{R}_{nm}$, where σ is the particle diameter and $\hat{R}_{nm}$ the unit vector from n to m. Set the nondiagonal terms $H(\vec{R}_m,\vec{R}_n)=k\hat{R}_{nm}\otimes\hat{R}_{nm}$, where k is the contact stiffness. With this substitution, Eq. (41) can be rewritten as a sum on all contacts $\langle n,m\rangle$:

$$S_{ij} = \frac{ih\sigma k}{2VM}\sum_{\langle n,m\rangle} \hat{R}_{nm}[(\vec{e}(n,i)\cdot\hat{R}_{nm})(\vec{e}(m,j)\cdot\hat{R}_{nm})$$

$$- (\vec{e}(n,j)\cdot\hat{R}_{nm})(\vec{e}(m,i)\cdot\hat{R}_{nm})]. \qquad (42)$$

We can then rewrite the sum in Eq. (42) as:

$$\Sigma(\omega) = \sum_{\langle n,m \rangle} \hat{R}_{nm}[(\vec{e}(n,i) \cdot \hat{R}_{nm} - \vec{e}(m,i) \cdot \hat{R}_{nm})(\vec{e}(m,j) \cdot \hat{R}_{nm})$$

$$- (\vec{e}(n,j) \cdot \hat{R}_{nm} - \vec{e}(m,j) \cdot \hat{R}_{nm})(\vec{e}(m,i) \cdot \hat{R}_{nm})], \quad (43)$$

and

$$\Sigma(\omega) = \sum_{\langle n,m \rangle} \hat{R}_{nm}[(\delta r_{nm}^i)(\vec{e}(m,j) \cdot \hat{R}_{nm}) - (\delta r_{nm}^j)(\vec{e}(m,i) \cdot \hat{R}_{nm})],$$
$$(44)$$

where $\delta r_{nm}^i \equiv (\vec{e}(n,i) \cdot \hat{R}_{nm} - \vec{e}(m,i) \cdot \hat{R}_{nm})$ is the stretching of the contact nm corresponding to mode i. Taking the amplitude squared of Σ leads to diagonal and nondiagonal terms. The latter are of two forms:

$$(\delta r_{nm}^i \hat{R}_{nm})(\delta r_{pq}^i \hat{R}_{pq})(\vec{e}(m,j) \cdot \hat{R}_{nm})(\vec{e}(q,j) \cdot \hat{R}_{pq}), \quad (45)$$

$$(\delta r_{nm}^i \hat{R}_{nm})(\delta r_{pq}^j \hat{R}_{pq})(\vec{e}(m,j) \cdot \hat{R}_{nm})(\vec{e}(p,i) \cdot \hat{R}_{pq}), \quad (46)$$

where nm and pq correspond to two distinct contacts.

We now make some assumptions about the nature of the modes whose validity we test numerically. (i) If the displacements are uncorrelated between different modes ($\langle \vec{e}(m,j) \cdot \vec{e}(q,i) \rangle = 0$), the two terms above become:

$$\langle (\delta r_{nm}^i \hat{R}_{nm})(\delta r_{pq}^i \vec{n}_{pq}) \rangle \langle (\vec{e}(m,j) \cdot \hat{R}_{nm})(\vec{e}(q,j) \cdot \hat{R}_{pq}) \rangle, \quad (47)$$

$$\langle (\delta r_{nm}^i \hat{R}_{nm})(\vec{e}(q,i) \cdot \hat{R}_{pq}) \rangle \langle (\vec{e}(m,j) \cdot \hat{R}_{nm})(\delta r_{pq}^j \hat{R}_{pq}) \rangle.$$
$$(48)$$

This assumption was tested numerically in a packing comprised of $N=2000$ particles at $\Delta\phi=10^{-6}$ for the low-frequency modes. Each of the two terms was found to be of the order of 10^{-21} which is vanishingly small within numerical precision.

We next assume that modes have weak spatial correlations. Numerical simulations actually support that such correlations exist [63] and grow as the frequency decreases. Neglecting them nevertheless appears to yield good quantitative results, as we shall see below. In particular, each of these two terms in Eq. (47) vanish under the specific assumptions that (ii) the directions of the stretching of different contacts within a mode are not correlated in space ($\langle (\delta r_{nm}^i \hat{R}_{nm})(\delta r_{pq}^i \hat{R}_{pq}) \rangle = 0$) and that (iii) the directions of stretching and of displacement are locally uncorrelated ($\langle (\delta r_{nm}^i \hat{R}_{nm})(\vec{e}(q,i) \cdot \hat{R}_{pq}) \rangle = 0$). For assumption (ii) we find that the corresponding terms are of the order of 10^{-11} or lower. For assumption (iii) we find a term of the order of 10^{-13} or less. If the quantities were correlated, we should find that for extended modes they are of the order of $1/N \approx 10^{-4}$, which is much larger than the values shown above. Therefore, the assumptions listed above appear to be reasonable and we are left with

$$|\Sigma|^2 \approx 2 \sum_{\langle n,m \rangle} \delta r_{nm}^{i\,2}(\vec{e}(m,j) \cdot \hat{R}_{nm})^2. \quad (49)$$

Assuming now that (iv) the amplitude of the displacements between two modes are not correlated (which does not apply

to localized modes, where the displacements are anticorrelated since localized modes do not live on the same regions of space) then we have:

$$|\Sigma|^2 = 2 \sum_{\langle n,m \rangle} \langle \delta r_{nm}^{i\,2} \rangle \langle (\vec{e}(m,j) \cdot \hat{R}_{nm})^2 \rangle. \quad (50)$$

The modes are normalized so $\langle (\vec{e}(m,j) \cdot \hat{R}_{nm})^2 \rangle = 1/N\mathcal{D}$, where $\mathcal{D}$ is the dimensionality of space. Also, the mode energy is $\delta E = M\omega^2/2 \equiv k/2 \sum_{\langle n,m \rangle} \delta r_{nm}^{i\,2}$, so we obtain

$$\Sigma = \frac{2M\omega^2}{k} \frac{1}{N\mathcal{D}}. \quad (51)$$

Then we have for Eq. (42)

$$|S|^2 = \frac{h^2 \omega^2 \sigma^2 k}{2V^2 \mathcal{D} N}. \quad (52)$$

This leads to

$$d(\omega) = \frac{\pi D(\omega) \sigma^2 k}{3m\mathcal{D}}. \quad (53)$$

where $D(\omega)$ is the density of states per particle. In units where $\sigma = k = m = 1$, we obtain

$$d_0 = \frac{\pi D_0}{9}, \quad (54)$$

in three dimensions, where d_0 and D_0 denote the plateau values of the diffusivity and the density of states, respectively. This is consistent with the numerical data in Fig. 5(d), which shows that the diffusivity roughly follows the nearly flat density of states at point J.

In summary, we obtain a frequency-independent diffusivity when the density of states is frequency-independent and the following conditions are satisfied: (A) displacements of particles in different modes of similar frequency are uncorrelated; (B) the directions of changes in the relative displacements of pairs of interacting particles are spatially uncorrelated within a given mode; and (C) the direction of change in the relative displacement of a pair of interacting particles is uncorrelated from the direction of the displacement.

C. Stressed packings

Until now, we have neglected the forces that particles within a jammed packing exert on each other by replacing compressed springs between particles with springs at their equilibrium length (see Sec. III B). Here we restore the stress terms into the dynamical matrix and examine how they affect the behavior. The scatter plot of the diffusivity of stressed samples shown as (black) dots in Fig. 6, plateaus at the same value d_0 observed in unstressed samples, shown as (red) crosses. However, the low ω upturn of the diffusivity that occurs below ω_d in the unstressed packing, is not clearly detected in the stressed data.

According to Eq. (23), the stress term, $V'(r)$, lowers the energy and frequency of each vibrational mode because $V'(r)$ is negative for repulsive interactions. As a result, finite-size effects, which cut-off plane waves at low frequencies,
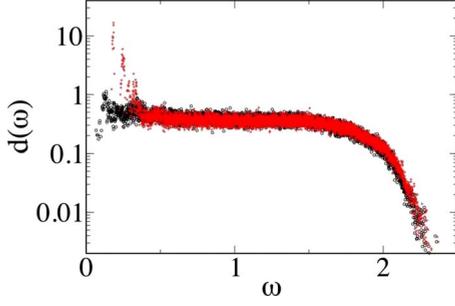
FIG. 6. (Color online) Diffusivity for $\Delta\phi = 0.1$ in stressed (black circles) and unstressed (red crosses) packings composed of 1000 particles with harmonic repulsions.

are more obstructive because the corresponding wavelengths exceed the system size. This prevents us from studying the packing fraction dependence of the transport crossover frequency ω_d directly in stressed systems and to test the validity of Eq. (37) [68].

Nevertheless, we note that the scaling of ω_d with compression should be the same in the stressed case as in the unstressed one if ω_d remains proportional to ω^*. This follows from the fact that the boson peak frequency, ω^*, follows the same power law [Eq. (12)] as in the unstressed case. This is illustrated in Fig. 7, which shows that the low-frequency portion of the vibrational spectrum collapses onto a single curve when ω is scaled by $\omega^* \sim \Delta\phi^{1/2}$ for harmonic repulsions.

VI. AC THERMAL CONDUCTIVITY AT POINT *J*

The calculation of the energy-flux matrix elements in Eq. (40) opens up the possibility of estimating the thermal conductivity $\kappa(T, \Omega)$ of the marginally jammed solid at point J, in the presence of an ac thermal gradient driven with angular frequency Ω. As a starting point we rewrite Eq. (16) as an integral over ω rather than a double sum over eigenmodes

$$\kappa(T, \Omega) = -\frac{\pi V}{T\Omega} \int [n(\omega + \Omega) - n(\omega)] |\langle \omega + \Omega | S | \omega \rangle|^2$$
$$\times D(\omega) D(\omega + \Omega) d\omega. \quad (55)$$

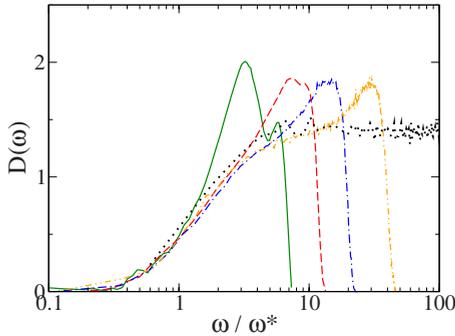where the frequency averaged matrix elements read

FIG. 7. (Color online) Density of states $D(\omega)$ vs ω / ω^* for $\Delta\phi = 0.0001$ (black dotted), 0.01 (yellow dashed-dot-dot), 0.05 (blue dot-dashed), 0.1 (red dashed) and 0.3 (green solid), for a stressed system with $N = 2000$ with harmonic repulsions. Note that ω^* scales according to Eq. (12). This scaling produces a good collapse of the vibrational spectrum at low frequency.

$$|\langle \omega + \Omega | S | \omega \rangle|^2 = \frac{(2\omega + \Omega)^2}{4\omega(\omega + \Omega)} |\Sigma(\Omega + \omega, \omega)|^2, \quad (56)$$

$$\approx \frac{\omega^2}{N}\left(1 + \frac{2\Omega}{\omega}\right), \quad (57)$$

and higher order corrections in terms of Ω^2 have been dropped. The prefactor in Eq. (20), which was set to unity in evaluating $\Sigma(\omega, \omega')$, has been explicitly included since the mode coupling between ω and ω' is no longer restricted to vibrational states at the same frequency. Despite the concise notation adopted, Eq. (55) accounts for both upwards and downwards jumps, $\omega \to \omega \pm \Omega$, corresponding to energy being absorbed or injected into the reservoirs [69]. In order to obtain Eq. (57), Eq. (40) was substituted into Eq. (56).

With the aid of Eq. (18), we can expand the difference in occupation numbers to first order in Ω

$$\frac{n(\omega + \Omega) - n(\omega)}{\Omega} \sim -\frac{T}{\hbar\omega^2}C(\omega) - \Omega\frac{\partial}{\partial\omega}\left[\frac{T}{\hbar\omega^2}C(\omega)\right]. \quad (58)$$

Upon substituting Eqs. (58) and (57) into Eq. (55), four terms are obtained of which one is $\mathcal{O}(\Omega^2)$ and it will be ignored. After performing an integration by parts on the $\mathcal{O}(\Omega)$ term involving the ω derivative and canceling out two terms which are equal and opposite, we obtain

$$\frac{\hbar\kappa(T, \Omega)}{\pi c_0 N_0^2} \approx \int_0^{\omega_{max}} C(\omega)d\omega + \Omega[C(\omega)]_0^{\omega_{max}}, \quad (59)$$

where N_0 is the value of the plateau in the density of states.

The desired result follows, according to Eq. (18), upon setting $C(\omega_{max} = \infty) \approx 0$

$$\kappa(T, \Omega) \approx \frac{\pi c_0 N_0^2 k_B^2}{\hbar^2}\left(\alpha T - \frac{\hbar\Omega}{k_B}\right) + \mathcal{O}(\Omega^2), \quad (60)$$

where the numerical constant α is given by

$$\alpha \approx \int_0^\infty \frac{x^2 e^x}{(e^x - 1)^2}dx. \quad (61)$$

As expected intuitively, a nonvanishing driving frequency Ω results in a lower thermal conductivity.

Equation (60) allows the calculation of the T-dependent dc thermal conductivity ($\Omega \to 0$) at point J. We note that this is particularly simple and can be calculated at the harmonic level without facing any divergences because no acoustic phonons are present, since ω_d is effectively shifted to zero. From Eq. (60), we find that $\kappa(T)$ grows linearly in temperature for small T and saturates above a temperature $k_B T_{max} \approx \hbar\omega_{max}$, where ω_{max} is the maximum frequency above which there are no more vibrational states. This follows from assuming that both the density of states and the diffusivity are approximately ω independent as expected from the scaling analysis and numerical extrapolations presented in Sec. IV A. Thus, a plateau in the diffusivity leads to an approximately linear increase of $\kappa(T)$ followed by a saturation.

VII. CONCLUSION

We have studied a class of model amorphous solids whose elastic properties can be tuned by varying the density near the jamming/unjamming transition, point J. The proximity to point J allows variation in the crossover frequency that marks the onset of the plateau in the diffusivity, ω_d, with $\Delta\phi$. As $\Delta\phi \to 0$, our scaling arguments show that $\omega_d \to 0$, so that the plateau in the diffusivity extends all the way down to zero frequency. Moreover, the value of ω_d agrees (within a factor close to unity) with the boson peak frequency ω^* that marks the onset of the excess vibrational modes in the density of states. Both ω_d and ω^* scale the same way with $\Delta\phi$.

The findings presented in this study enable us to establish that there is a frequency regime in which the diffusivity is small and nearly constant, and that the boson peak frequency coincides with the energy transport crossover frequency for all pressures applied to our unstressed amorphous packings of repulsive spheres. More work is needed to assess the relationship between the boson peak and the transport crossover when prestress is important. Nonetheless, our results suggest solutions to two conundrums posed by these amorphous solids. First, in such systems, the plateau in the thermal conductivity at intermediate temperatures is followed by a rise and then a saturation at high temperatures unlike crystals that show the opposite behavior, with a thermal conductivity that decreases with T at high T, see Fig. 5.1 in Ref. [2]. Second, the temperature range of the plateau in the thermal conductivity lies near the temperature at which the heat capacity exhibits a boson peak.

The answer to the first conundrum follows naturally from our result that there is a frequency regime of small and constant diffusivity. As shown in Sec. VI, the plateau in the diffusivity above ω_d gives rise to a linear increase in thermal conductivity above $k_B T_d \sim \hbar\omega_d$. Similarly, the vanishing of the density of states at $\omega_{\max}$ leads to saturation of $\kappa(T)$ at high $k_B T > \hbar\omega_{\max}$. Thus, the transport crossover frequency sets the high-temperature limit of the plateau in $\kappa(T)$, while the maximum allowed frequency sets the temperature at which $\kappa(T)$ saturates to its final high-temperature value.

The answer to the second conundrum follows directly from the observation that $\omega_d \approx \omega^*$, since the high-temperature limit of the plateau in $\kappa(T)$ is $k_B T_d \sim \hbar\omega_d$ and the boson peak temperature is $k_B T_{BP} \sim \hbar\omega^*$. Therefore, $T_d \approx T_{BP}$.

Our results were obtained for a special system in which spheres interact via finite-ranged repulsions. Nonetheless, it

has been argued theoretically [47] and shown numerically [61] that packings of spheres interacting via Lennard-Jones interactions, which are attractive at long distances, behave much as compressed packings of repulsive spheres and that the boson peak frequency shifts upwards with increasing density in such systems. Indeed, it was found that the ω^* is determined primarily by the repulsive interactions that come into play because the systems are held at high densities by the attractions. Thus, even systems with attractions display a boson peak corresponding to the onset of anomalous modes, which should lead to a transport crossover as well.

It has also been shown that packings of ellipsoids [70] display boson peaks corresponding to the onset of anomalous modes that are similar in character to those for spheres. For ellipsoids, the boson peak frequency is controlled by much the same physics as for spheres; it depends on the coordination number as in Eq. (36).

Another class of systems, network glasses, appears at first glance to be very different from our model repulsive sphere packings. However, the unstressed models that were the main focus of this paper can be described as points (corresponding to the centers of spheres) connected by unstretched springs. Such networks bear some resemblance to network glasses, which are held together by covalent attractions. We include only central forces, but the counting of constraints has been shown to be key to network glasses with bond-bending forces as well [71,72]. The connection between harmonic spring networks and covalent network glasses has been discussed in more detail in Refs. [47,73].

In summary, our results suggest that two generic features of amorphous solids, the rise of the thermal conductivity with temperature above a plateau and the coincidence of the plateau temperature with the boson peak temperature, can be traced to the presence of strongly scattered vibrational modes with constant, minimal diffusivity. In the amorphous packings of soft spheres considered in our study, the unjamming transition controls the frequency onset of these anomalous vibrational modes in the manner of a critical point.

[1] S. R. Elliott, *Physics of Amorphous Materials* (Longman, Harlow, 1990), pp. 222–243.

[2] *Amorphous Solids in Low Temperature Properties*, edited by W. A. Phillips (Springer-Verlag, Berlin, 1981).

[3] V. Lubchenko and P. G. Wolynes, Proc. Natl. Acad. Sci. U.S.A. **100**, 1515 (2003).

[4] P. Sheng and M. Zhou, Science **253**, 539 (1991).

[5] P. B. Allen and J. L. Feldman, Phys. Rev. B **48**, 12581 (1993); J. L. Feldman, P. B. Allen, and S. R. Bickham, *ibid.* **59**, 3551 (1999).

[6] D. G. Cahill and R. O. Pohl, Phys. Rev. B **35**, 4067 (1987).

[7] A. C. Anderson, in *Amorphous Solids. Low Temperature Properties*, edited by W. A. Phillips (Springer-Verlag, Berlin, 1981).

[8] X. Liu and H. v. Lšhneysen, Europhys. Lett. **33**, 617 (1996).

[9] R. C. Zeller and R. O. Pohl, Phys. Rev. B **4**, 2029 (1971).

[10] S. R. Nagel, G. S. Grest, S. Feng, and L. M. Schwartz, Phys. Rev. B **34**, 8667 (1986).

[11] P. W. Anderson, B. I. Halperin, and C. M. Varma, Philos. Mag. **25**, 1 (1972).

[12] R. O. Pohl, X. Liu, and E. Thompson, Rev. Mod. Phys. **74**, 991 (2002).

[13] C. S. O'Hern, L. E. Silbert, A. J. Liu, and S. R. Nagel, Phys. Rev. E **68**, 011306 (2003).

[14] L. E. Silbert, A. J. Liu, and S. R. Nagel, Phys. Rev. Lett. **95**, 098301 (2005).

[15] N. Xu, V. Vitelli, M. Wyart, A. J. Liu, and S. R. Nagel, Phys. Rev. Lett. **102**, 038001 (2009).

[16] B. B. Laird and H. R. Schober, Phys. Rev. Lett. **66**, 636 (1991).

[17] H. R. Schober and C. Oligschleger, Phys. Rev. B **53**, 11469 (1996).

[18] R. Biswas, A. M. Bouchard, W. A. Kamitakahara, G. S. Grest, and C. M. Soukoulis, Phys. Rev. Lett. **60**, 2280 (1988).

[19] A. L. Burin, L. A. Maksimov, and I. Ya. Polishchuk, Physica B **210**, 49 (1995).

[20] D. Caprion, P. Jund, and R. Jullien, Phys. Rev. Lett. **77**, 675 (1996).

[21] V. G. Karpov, M. I. Klinger, and F. N. Ignatiev, Sov. Phys. JETP **57**, 439 (1983).

[22] U. Buchenau, Yu. M. Galperin, V. L. Gurevich, D. A. Parshin, M. A. Ramos, and H. R. Schober, Phys. Rev. B **46**, 2798 (1992).

[23] M. Wyart, S. R. Nagel, and T. A. Witten, Europhys. Lett. **72**, 486 (2005).

[24] J. P. Wittmer, A. Tanguy, J. L. Barrat, and L. Lewis, Europhys. Lett. **57**, 423 (2002).

[25] S. R. Elliott, Europhys. Lett. **19**, 201 (1992).

[26] W. Schirmacher, Europhys. Lett. **73**, 892 (2006).

[27] W. Schirmacher, G. Ruocco, and T. Scopigno, Phys. Rev. Lett. **98**, 025501 (2007).

[28] W. Schirmacher, G. Diezemann, and C. Ganter, Phys. Rev. Lett. **81**, 136 (1998).

[29] D. A. Parshin and C. Laermans, Phys. Rev. B **63**, 132203 (2001).

[30] C. Masciovecchio, G. Ruocco, F. Sette, M. Krisch, R. Verbeni, U. Bergmann, and M. Soltwisch, Phys. Rev. Lett. **76**, 3356 (1996).

[31] M. Foret, E. Courtens, R. Vacher, and J.-B. Suck, Phys. Rev. Lett. **77**, 3831 (1996).

[32] B. Ruffle, G. Guimbretiere, E. Courtens, R. Vacher, and G. Monaco, Phys. Rev. Lett. **96**, 045502 (2006).

[33] T. Scopigno, J. B. Suck, R. Angelini, F. Albergamo, and G. Ruocco, Phys. Rev. Lett. **96**, 135501 (2006).

[34] G. Winterling, Phys. Rev. B **12**, 2432 (1975).

[35] R. J. Nemanich, Phys. Rev. B **16**, 1655 (1977).

[36] O. Pilla *et al.*, J. Phys.: Condens. Matter **16**, 8519 (2004).

[37] J. Horbach, W. Kob, and K. Binder, Eur. Phys. J. B **19**, 531 (2001).

[38] H. R. Schober, J. Phys.: Condens. Matter **16**, S2659 (2004).

[39] H. Shintani and H. Tanaka, Nat. Mater. **7**, 870 (2008).

[40] C. Kittel, Phys. Rev. **75**, 972 (1949).

[41] S. John, H. Sompolinsky, and M. J. Stephen, Phys. Rev. B **27**, 5592 (1983).

[42] R. J. Hemley, C. Meade, and H. K. Mao, Phys. Rev. Lett. **79**, 1420 (1997).

[43] V. L. Gurevich, D. A. Parshin, and H. R. Schober, Phys. Rev. B **71**, 014209 (2005) and references therein.

[44] P. Sheng, *Introduction to Wave Scattering, Localization and Mesoscopic Phenomena* (Springer-Verlag, New York, 2006).

[45] D. J. Durian, Phys. Rev. Lett. **75**, 4780 (1995).

[46] S. Alexander, Phys. Rep. **296**, 65 (1998).

[47] M. Wyart, Ann. Phys. (Paris) **30**, 1 (2005).

[48] P. W. Anderson, Phys. Rev. **109**, 1492 (1958).

[49] N. W. Ashcroft and D. N. Mermin, *Solid State Physics* (Brooks Cole, New York, 1976).

[50] P. A. Lee and D. S. Fisher, Phys. Rev. Lett. **47**, 882 (1981).

[51] E. Akkermans, *Mesoscopic Physics of Electrons and Photons* (Cambridge University Press, Cambridge, 2007).

[52] *Thermal conductivity: Theory, Properties, and Applications*, edited by T. M. Tritt (Springer-Verlag, Berlin, 2005).

[53] J. E. Graebner, B. Golding, and L. C. Allen, Phys. Rev. B **34**, 5696 (1986).

[54] M. Wyart, L. E. Silbert, S. R. Nagel, and T. A. Witten, Phys. Rev. E **72**, 051306 (2005).

[55] F. Leonforte, A. Tanguy, J. P. Wittmer, and J.-L. Barrat, Phys. Rev. Lett. **97**, 055501 (2006).

[56] F. Leonforte, R. Boissiere, A. Tanguy, J. P. Wittmer, and J.-L. Barrat, Phys. Rev. B **72**, 224206 (2005).

[57] It corresponds to one over the number of dimensions if the deformations induced in the packing upon compression are affine.

[58] P. Jund and R. Jullien, Phys. Rev. B **59**, 13707 (1999).

[59] G. A. Slack, in *Solid State Physics*, edited by F. Seitz, D. Turnbull, and H. Ehrenreich (Academic Press, New York, 1979), Vol. 34, p. 1.

[60] M. Wyart, e-print arXiv:0909.3030.

[61] N. Xu, M. Wyart, A. J. Liu, and S. R. Nagel, Phys. Rev. Lett. **98**, 175502 (2007).

[62] G. S. Grest, S. R. Nagel, and A. Rahman, Phys. Rev. Lett. **49**, 1271 (1982).

[63] L. E. Silbert, A. J. Liu, and S. R. Nagel, Phys. Rev. E **79**, 021308 (2009).

[64] Z. Zeravcic, W. van Saarloos, and D. R. Nelson, Europhys. Lett. **83**, 44001 (2008).

[65] S. R. Nagel, A. Rahman, and G. S. Grest, Phys. Rev. Lett. **47**, 1665 (1981).

[66] S. R. Nagel, G. S. Grest, and A. Rahman, Phys. Rev. Lett. **53**, 368 (1984).

[67] W. G. Ellenbroek, E. Somfai, M. van Hecke, and W. van Saarloos, Phys. Rev. Lett. **97**, 258001 (2006).

[68] Note that the shear modulus of stressed samples has the same packing fraction dependence of the unstressed ones but it is lower by a factor of 2 approximately.

[69] N. F. Mott and E. A. Davis, *Electronic Processes in Non-Crystalline materials* (Clarendon Press, Oxford, 1971), pp. 10–14.

[70] Z. Zeravcic, N. Xu, A. J. Liu, S. R. Nagel, and W. van Saarloos, Europhys. Lett. **87**, 26001 (2009).

[71] J. C. Phillips, J. Non-Cryst. Solids **43**, 37 (1981).

[72] M. F. Thorpe, J. Non-Cryst. Solids **57**, 355 (1983).

[73] M. Wyart, H. Liang, A. Kabla, and L. Mahadevan, Phys. Rev. Lett. **101**, 215501 (2008).